Description of the thermalization process of the sputtered atoms in a glow discharge using a three-dimensional Monte Carlo method

Annemie Bogaerts,[a] Mark van Straaten, and Renaat Gijbels
Department of Chemistry, University of Antwerp, Universiteitsplein 1, B-2610 Wilrijk-Antwerpen, Belgium

(Received 4 October 1994; accepted for publication 21 November 1994)

A three-dimensional Monte Carlo model is developed to simulate the thermalization process of atoms sputtered from the cathode in a glow discharge cell. A comparison is made with a simplified analytical thermalization model and the relative importance of different interaction potentials and scattering assumptions on quantities related to thermalization is investigated. Typical results of the thermalization model are (i) the thermalization profile (which gives the distribution of the thermalized sputtered atoms), (ii) the relative amount of atoms that can reach the backplate of the discharge cell without being thermalized, and (iii) the relative amount of backscattering to the cathode. The influence of gas pressure, kind of gas, and cathode material on the thermalization process is also investigated. © *1995 American Institute of Physics.*

I. INTRODUCTION

A glow discharge consists of two electrodes inserted into a low-pressure inert gas environment (10–1000 Pa). A voltage of 200–2000 V is applied between the electrodes and causes electrical breakdown of the gas, producing positive ions and electrons. The positive ions are accelerated towards the cathode by the potential drop and cause the emission of secondary electrons upon impact. These electrons are accelerated away from the cathode giving elastic and inelastic (excitation and ionization) collisions in the glow discharge plasma. The ionization collisions create new ions and electrons, which assures the maintenance of the glow discharge. The ion bombardment on the cathode also induces a collision cascade in the cathode material, with energy sufficient to release one or more atoms per incoming ion from its surface. These sputtered atoms are liberated into the plasma and can become ionized or excited, making the glow discharge applicable as an analytical source for elemental mass spectrometry and optical emission spectrometry.[1–3]

To improve our understanding of the analytical results achieved with these techniques, an insight in the fundamental processes of the glow discharge is necessary. This insight can be acquired by theoretical modeling. Modeling of a glow discharge is a combination of two kinds of models, a plasma model[4–6] which describes the behavior of electrons, gas ions, and fast gas atoms (i.e., the plasma species) and a sputter model[7–10] which describes the behavior of the sputtered atoms and is linked to the results of the plasma model by the sputter bombardment of gas ions and fast gas atoms on the cathode. A sputter model will be considered here.

The atoms sputtered from the cathode enter into the plasma with initial energies of about 5–15 eV.[3] They first lose these initial energies by elastic collisions with the gas atoms and then diffuse further into the plasma or back to the cathode. Because the thermalization process is much faster than the diffusion process, it can be assumed already finished when the diffusion starts.[8] Hence it is possible to separate both processes in time when modeling the behavior of the sputtered atoms.[8] In this paper, we will first simulate the thermalization process of the atoms, resulting in a thermalization profile, and in a later work, this thermalization profile will be used as the starting condition for the diffusion process.

Gras-Marti and Valles-Abarca[7,8] have described a simplified model which solves the thermalization process analytically. They used an approximate power-law potential with constant power n to describe the interatomic interactions and assumed that the sputtered atoms move along a straight line (one-dimensional model) and lose their energy in a continuous manner (continuous slowing down approximation) instead of considering the energy loss explicitly in each collision and dependent on the scattering conditions of the collision. In the present work, a three-dimensional Monte Carlo model is developed, which allows us to describe the problem explicitly on an atomic scale. We followed the three-dimensional trajectory of each sputtered atom separately and calculated the scattering angle and the energy loss if a collision took place. We also used a more accurate screened Coulomb potential to describe the collision interactions. For comparison with the analytically solvable model,[7,8,10] the Monte Carlo simulations were also carried out in a simplified one-dimensional way and the differences due to different choices of interaction potentials and scattering conditions were investigated.

II. DESCRIPTION OF THE MODEL

Thermalization of sputtered atoms is based on elastic collisions with gas atoms. Accurate description of collisions between atoms requires a knowledge of the interaction potential between these atoms because this determines the cross section, the scattering angles, and the energy loss in a collision. A variety of different interaction potentials between atoms can be found in the literature.[11,12] The screened Coulomb potentials present a realistic view of atomic interactions.[11] They are based on the Thomas–Fermi model of an atom and represent a simple Coulomb repulsion between the atoms at very small distances of separation, com-

[a]Author to whom correspondence should be addressed; Electronic mail: bogaerts@uia.ua.ac.be

 0021-8979/95/77(5)/1868/7/$6.00

bined with a screening function to simulate the interaction between the atomic electrons, which makes itself felt at large separations:

$$V(r)=\frac{Z_1Z_2e^2}{r}f(r), \tag{1}$$

where Z_1 and Z_2 are the atomic numbers of the interacting atoms, r the distance of separation, and $f(r)$ the screening function.

Another way of describing the atomic interactions is given by the power-law potentials:[13]

$$V(r)=\frac{Z_1Z_2e^2a_s^{n-1}}{nr^n}, \tag{2}$$

where a_s is the screening radius (in angstroms) $=0.468/(\sqrt{Z_1}+\sqrt{Z_2})^{0.667}$ and n is a power, varying from 1 to about 16.

To describe the interatomic scattering collisions, Lindhard *et al.* derived the following differential cross section, dependent on the interaction potential:[14,15]

$$d\sigma=\pi a_s^2\frac{dt}{2t^{3/2}}f(t), \tag{3}$$

where

$$t=\left(\frac{m_2E}{(m_1+m_2)}\frac{a_s}{Z_1Z_2e^2}\right)^2\frac{T}{\gamma E}, \tag{4}$$

and E is the initial energy, T the recoil energy, $0\leq T\leq\gamma E$ (maximum recoil energy), $\gamma=4m_1m_2/(m_1+m_2)^2$, m_1 the mass of the scattered particle, m_2 the mass of the recoiling particle, and Z_1, Z_2, and a_s are explained before, $f(t)$ is a function that depends on the assumed interaction potential.

For a Thomas–Fermi screened Coulomb potential

$$f(t)=1.309t^{1/6}[1+(2.618t^{2/3})^{2/3}]^{-3/2}. \tag{5}$$

For a power-law potential

$$f(t)=\lambda_m t^{1/2-m}, \tag{6}$$

where $m=1/n$ and λ_m is a constant depending on m.

The differential cross section given in Eq. (3) can be used to analytically calculate certain quantities that are of importance for the description of the thermalization process,[13–17] like the energy loss per unit traveled path length, the range of the sputtered particles, and the thermalization profile itself. Gras-Marti and Valles-Abarca[7,8] used for this purpose the differential cross section for the power-law potential with constant power n because it allows fairly simple analytical solutions of the integral equations. However, the results are only approximate and have to be checked by more exact results. The differential cross section based on a screened Coulomb potential is more accurate but the mathematics of solving the integral equations are much more complicated. Therefore we did not solve the integral equations but developed a Monte Carlo model to simulate the thermalization process and used the latter, more exact, differential cross section to describe the interactions explicitly in each collision.

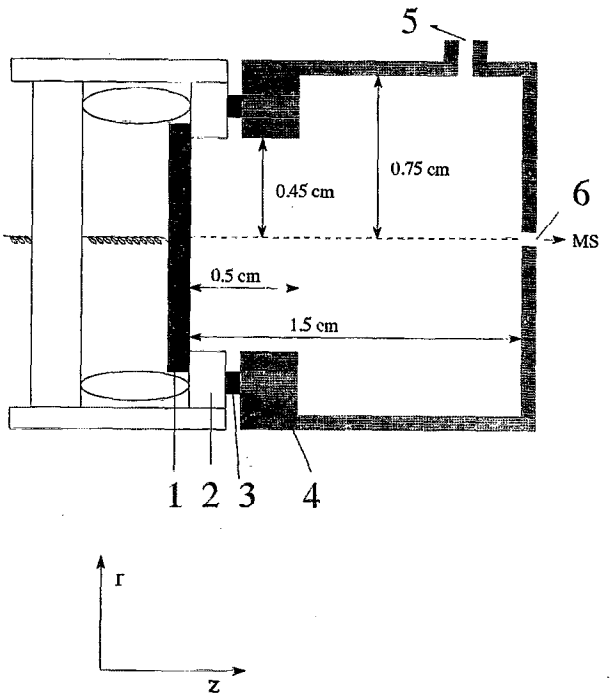

FIG. 1. Standard glow discharge cell in the VG 9000 mass spectrometer: (1) sample (cathode), (2) mask, (3) insulator, (4) cell body (anode), (5) gas inlet, and (6) exit slit.

The discharge we want to model relates to the standard discharge cell of a Fisons VG 9000 glow discharge mass spectrometer for analyzing flat samples.[18] This cell has a cylindrical geometry with a flat cathode (see Fig. 1). The calculations are carried out in three dimensions, but the final results of a statistically significant number of atoms are cylindrically symmetrical and can be presented in a two-dimensional way.

The sputtered atoms are leaving the cathode with an energy and angular distribution given by[8]

$$\Psi(E,\theta)=\frac{2UE}{(E+U)^3}\frac{\cos\theta}{\pi}, \tag{7}$$

where U is the surface binding energy of the cathode material, mostly taken equal to the sublimation energy, and θ is the angle of the velocity vector with respect to the axial direction.

Using random numbers (rn) between 0 and 1, the specific angle and energy of a sputtered atom starting at the cathode are calculated from Eq. (7) as

$$\begin{aligned} rn(\theta)&=\int_0^{\infty}dE'\int_0^{\theta}d\theta'\times 2\pi\sin(\theta')\times\Psi(E,\theta'),\\ rn(E)&=\int_0^{E}dE'\int_0^{\pi/2}d\theta'\times 2\pi\sin(\theta')\times\Psi(E,\theta'), \end{aligned} \tag{8}$$

which results in

$$\begin{aligned} &\theta=1/2\ \text{acos}(1-2rn),\\ &E^2(rn-1)+E(2Urn)+U^2rn=0, \end{aligned} \tag{9}$$

where the positive root gives E.

The azimuthal angle ϕ (i.e., the angle of the projection of the velocity vector in the xy plane, with respect to the x axis) is also determined by a random number between 0 and 1:

$$\phi = 2\pi rn. \tag{10}$$

The x and y coordinates of the starting position are also determined by random numbers. The starting z coordinate is zero.

The distance traveled by the atoms after a time step Δt is described by Newton's laws:

$$z = z_0 + v_{z_0}\Delta t, \quad x = x_0 + v_{x_0}\Delta t, \quad y = y_0 + v_{y_0}\Delta t, \tag{11}$$

where z_0, x_0, and y_0 are the position coordinates at $t = t_0$, z, x, and y the position coordinates at $t = t_0 + \Delta t$, and v_{z0}, v_{x0}, and v_{y0} the velocity components in the z, x, and y directions:

$$v_{z0} = 2E/m \times \cos\theta,$$

$$v_{x0} = 2E/m \times \sin\theta \cos\phi,$$

$$v_{y0} = 2E/m \times \sin\theta \sin\phi.$$

The probability P of a collision event during this time step Δt is given by

$$P = 1 - \exp[-n\sigma_{\text{ela}}(E)\Delta s], \tag{12}$$

where Δs is the distance traveled in the time step Δt {i.e., $\Delta s = [(z-z_0)^2 + (x-x_0)^2 + (y-y_0)^2]^{1/2}$} and σ_{ela} is the cross section of elastic collision with the gas atoms. Only this kind of collision is assumed, because it has by far the highest cross section and the density of gas atoms is much higher than that of any other species in the plasma. The elastic cross section as a function of the energy is determined by integrating the Lindhard's differential cross section $d\sigma$ over all possible energy losses dT:

$$\sigma_{\text{ela}}(E) = \int_0^{\gamma E} d\sigma. \tag{13}$$

Because the differential cross section $d\sigma$ for a screened Coulomb potential is rather complicated, its integration is facilitated by using the differential cross section for a power-law potential with varying the power n as a function of the energy to approximate the screened Coulomb potential[19] (and see further when the scattering angle is discussed):

$$\sigma(E) = nC\gamma^{-1/n}E^{-2/n}, \tag{14}$$

where

$$C = \frac{\pi}{2}\lambda_m a_s^2 \left(\frac{m_1}{m_2}\right)^{1/n} \left(\frac{2Z_1Z_2e^2}{a_s}\right)^{2/n},$$

$$\gamma = \frac{4m_1m_2}{(m_1+m_2)^2},$$

$$n = 1 + 4\exp(-1.9\epsilon^{0.1}), \tag{15}$$

$$\epsilon = \frac{m_2E}{m_1+m_2}\frac{a_s}{Z_1Z_2e^2},$$

and all parameters are explained before.

The probability of collision in Eq. (12) is compared with a random number in the [0,1] interval. If the probability is lower, no collision takes place and the atom follows its way during a new time step. If the probability is higher, a collision takes place and the new direction and energy after scattering have to be determined.

The description of the scattering event depends on the kind of interaction potential considered. In this model, we assume a screened Coulomb potential [see Eq. (1)], i.e., the Molier potential, with a screening function given by

$$f(r) = 0.35e^{-0.3r/a_s} + 0.55e^{-1.2r/a_s} + 0.1e^{-6r/a_s}. \tag{16}$$

Sielanko[19] has derived an analytical expression for the scattering angle in the center-of-mass frame of reference χ_{com} using Lindhard's differential cross section for a power-law potential approximating the Molier potential by choosing the parameters n and K_n as a function of the energy and the impact parameter:

$$\sin^2\left(\frac{\chi_{\text{com}}}{2}\right) = \left(1 + \frac{p^2\epsilon^{2/n}}{(K_n^2\beta_n^2)^{1/n}}\right)^{-n}. \tag{17}$$

The complete description of this formula is found in Ref. 19. The impact parameter is calculated from the cross section using a random number between 0 and 1.[20] The conversion of the scattering angle into the laboratory frame of reference χ_{lab} is achieved by[12]

$$\tan\chi_{\text{lab}} = \frac{\sin\chi_{\text{com}}}{m_1/m_2 + \cos\chi_{\text{com}}}, \tag{18}$$

where m_1 and m_2 are the masses of the sputtered and gas atoms, respectively.

The azimuthal angle of scattering Ψ is determined by a random number:

$$\Psi = 2\pi rn. \tag{19}$$

The new energy E depends on the scattering angle and is given by[19]

$$E = E_0\left(1 - \sin^2\frac{\chi_{\text{com}}}{2}\right), \tag{20}$$

where E_0 is the energy before collision.

The new direction in the three-dimensional space, i.e., the new angles θ and ϕ, are calculated from the angles θ_0 and ϕ_0 before scattering and from the scattering angle χ and the azimuthal angle of scattering Ψ, by transformation of the coordinate frame of reference (see Fig. 2):

$$\begin{pmatrix} \sin(\theta)\cos(\phi) \\ \sin(\theta)\sin(\phi) \\ \cos(\theta) \end{pmatrix} = \begin{pmatrix} \cos(\theta_0)\cos(\phi_0) & -\sin(\phi_0) & \sin(\theta_0)\cos(\phi_0) \\ \cos(\theta_0)\sin(\phi_0) & \cos(\phi_0) & \sin(\theta_0)\sin(\phi_0) \\ -\sin(\theta_0) & 0 & \cos(\theta_0) \end{pmatrix} \times \begin{pmatrix} \sin(\chi)\cos(\Psi) \\ \sin(\chi)\sin(\Psi) \\ \cos(\chi) \end{pmatrix}. \tag{21}$$

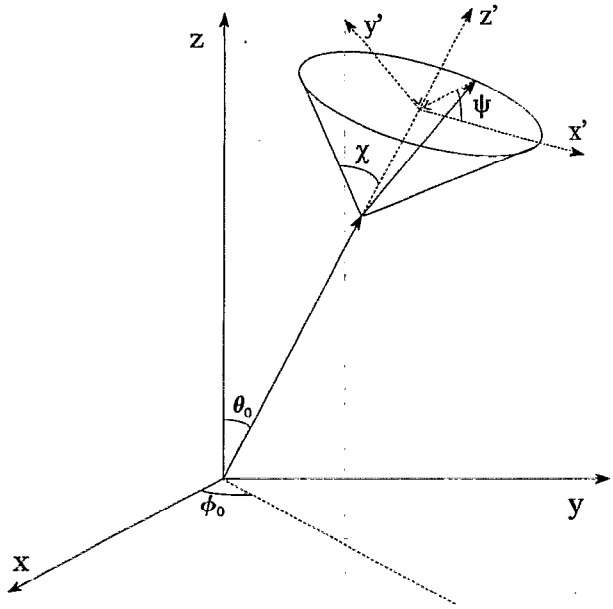

FIG. 2. Definition of the two frames of reference and the different angles in the three-dimensional system: xyz=laboratory frame of reference, $x'y'z'$=particle scattering frame of reference, θ_0 and ϕ_0=axial and azimuthal angle of the particle before scattering, and χ and Ψ = scattering angle and azimuthal angle of scattering.

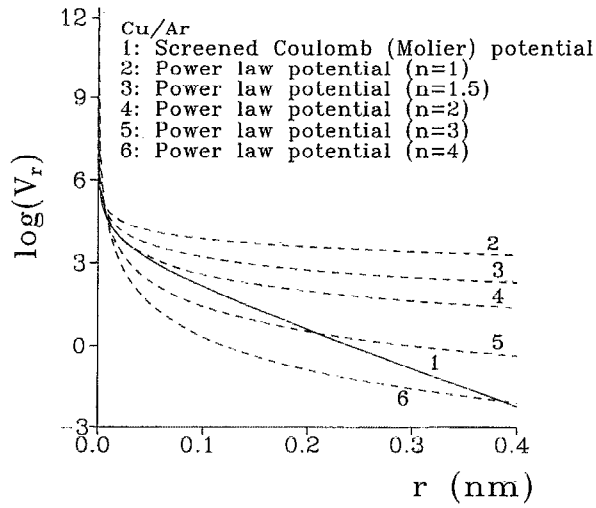

FIG. 3. Comparison of the Molier potential with different power-law potentials for interaction between Cu and Ar atoms.

After the new energy and direction are determined, the atom is followed during the next time step, and the procedure is repeated.

When the atoms collide at the walls of the cell, they can be adsorbed or reflected. Little is known about reflection or sticking coefficients for atoms with low energies. We have found data of reflection coefficients in the literature for kiloelectron-volt energies,[17] but it is not evident that these values can be extrapolated to the energies used here. We have carried out the calculations with reflection coefficients ranging from 0 to 1 and it does not seem to influence the shape of the thermalization profile; only the absolute value is slightly influenced. Hence we take as a first approximation a reflection coefficient equal to 0.5.

In the case of adsorption, the atom disappears from the plasma and the calculation stops. In the case of reflection, we assume that the atom is reflected back into the plasma without any change in energy and in a direction symmetrical with respect to the normal to the wall, as if pure elastic reflection has taken place.

The atoms are followed until they have thermal energies (i.e., $E<0.03$ eV). In this way the distribution of thermalized sputtered atoms in the discharge environment is obtained.

III. RESULTS AND DISCUSSION

A. Comparison of the interaction potentials and their influence on quantities important for the thermalization process

Figure 3 shows the comparison of the Molier (screened Coulomb) potential with power-law potentials for different values of the power n, for the interaction between a Cu and an Ar atom. It is clear that no single power-law potential closely approximates the Molier potential. The potential with power $n=2$ seems a good approximation for low values of r, power $n=3$ can be used for intermediate values of r, and power $n=4$, which was mostly used in Ref. 8, is suitable for higher values of r. Hence when describing an atomic interaction with a power-law potential, a different power n should be used depending on the energy of interaction [see Eq. (15)]. Indeed, for very low energies (about 0.01 eV), the atoms cannot approach each other very closely (large values of r), and n will be near to 4. When the energy increases, the atoms can come closer to each other and n will decrease. For energies of 10 eV, n will be about 3, and for energies of 1000 eV a value of nearly 2 will be reached.

This variable power n was used to calculate the cross section of elastic collisions. In Fig. 4 the cross section for an approximated Molier potential is compared with the cross section for a power-law potential with $n=4$, for the energies of importance for the thermalization process (i.e., 0.03–20 eV). For low energies, the agreement is of course reasonably good, but for energies in the range of 10 eV and more, the power-law cross section is more than 2× higher than the one based on the Molier potential.

Another important quantity for the thermalization process, which also depends on the kind of interaction potential, is the average energy lost in a collision. Figure 5 shows the average energy lost in a collision per unit energy for a power-law potential ($n=4$) and for the approximated Molier potential as a function of the energy. The energy loss in the case of a Molier potential is for all energies higher than in the case of a power-law potential, because the scattering angle is generally larger. A power-law potential gives an average energy loss independent of the energy, but an approximated Molier potential (n as a function of the energy) results in an increasing energy loss as a function of the energy; indeed, at high energies, the atom can approach closer, the impact parameter is smaller, and hence the scattering angle is

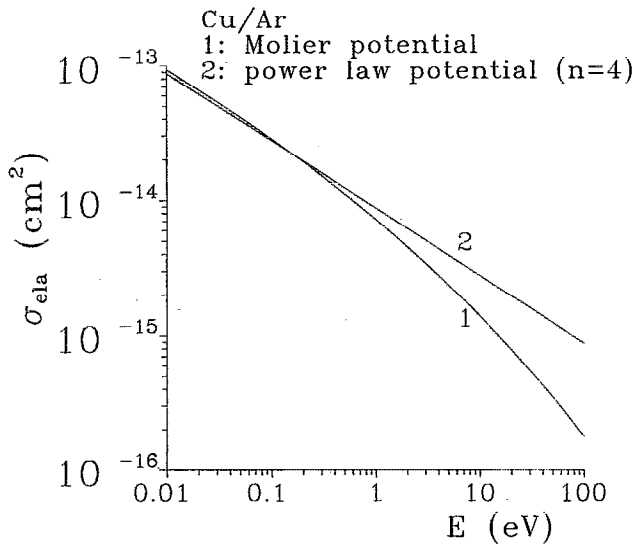

FIG. 4. Comparison of the Cu/Ar elastic cross section obtained by the approximated Molier potential and by a power-law potential ($n=4$), as a function of the energy.

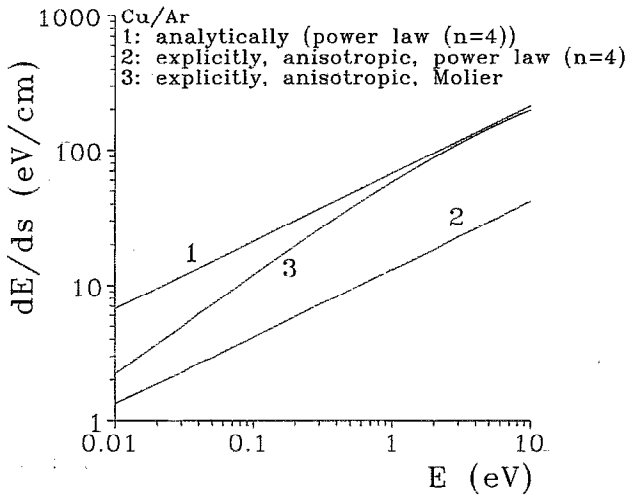

FIG. 6. Comparison of the energy lost per unit traveled path length for Cu/Ar, calculated analytically and explicitly with the Monte Carlo method for a Molier potential and for a power-law potential with $n=4$, as a function of the energy.

larger, resulting in more energy loss [see Eq. (20)]. We compared these values with the energy loss in isotropic scattering where all scattering angles are equally probable, independent of the energy ($\langle\chi_{com}\rangle=90°$), and the average energy loss per unit energy is given by[12]

$$\frac{\Delta E}{E}=\frac{\gamma}{2}=0.474 \quad \text{(for Cu/Ar)}. \tag{22}$$

For energies lower than about 3 eV, the average energy loss in the case of anisotropic scattering described by the Molier potential is lower than in the case of isotropic scattering, because the average scattering angle is in general lower. At higher energies, the situation is reversed.

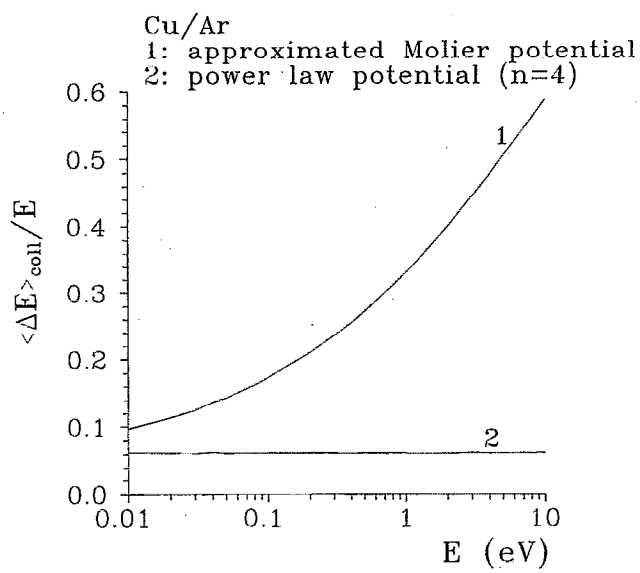

FIG. 5. Comparison of the average energy lost in a Cu/Ar collision per unit energy calculated with the approximated Molier potential and with a power-law potential ($n=4$), as a function of the energy.

With the average energy lost in a collision, we can calculate the energy lost per unit traveled path length—an important parameter in the analytical continuous slowing down model—by multiplying it with the number of collisions per unit path length ($n\sigma_{ela}$):

$$\frac{dE}{ds}=\langle\Delta E\rangle_{coll} n\times\sigma_{ela}. \tag{23}$$

Comparison of this parameter for the different scattering conditions with the analytical result [see Ref. 8 and Eq. (24)] leads to Fig. 6. The energy lost in the anisotropic cases is clearly lower than the analytically calculated energy loss, especially at low energies:

$$\frac{dE}{ds}=\frac{4}{3}\gamma^{3/4}nCE^{1/2}. \tag{24}$$

When we express the analytically evaluated parameter of Eq. (24) explicitly as the energy lost in a collision multiplied by the number of collisions per unit traveled path length [Eq. (23)], we find the energy lost in one collision to be equal to $E\gamma/3$ (i.e., 0.316 E for Cu/Ar):

$$\sigma_{ela}(E)=4C\gamma^{-1/4}E^{-1/2} \quad (\text{for } V\sim r^{-4}),$$

$$\Rightarrow\frac{dE}{ds}=\sigma_{ela}n\frac{\gamma}{3}E,$$

$$\Rightarrow\langle\Delta E\rangle_{coll}=\frac{\gamma}{3}E. \tag{25}$$

This value is slightly less than the isotropic energy loss ($E\gamma/2$, i.e., 0.474 E for Cu/Ar) and clearly higher than the anisotropic energy loss calculated with the power-law potential (see Fig. 5). Compared to the energy loss for the Molier

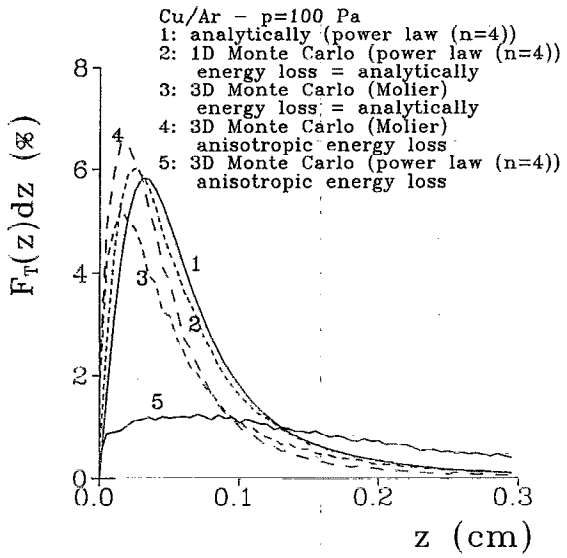

FIG. 7. Comparison of the thermalization profile for Cu atoms in Ar at 100 Pa, calculated for different potentials and scattering assumptions.

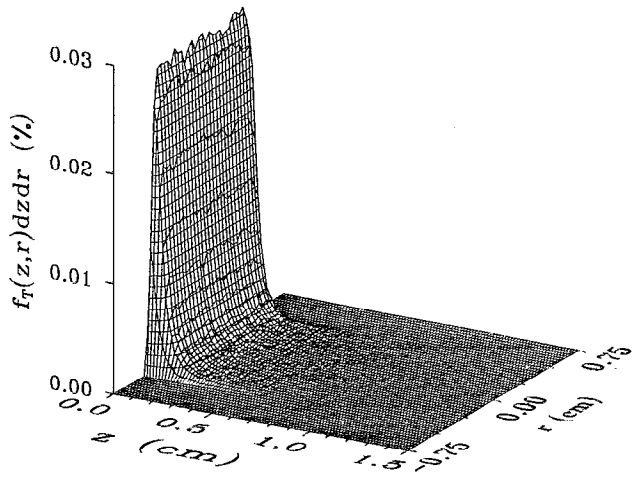

FIG. 8. Thermalization profile for Cu atoms in Ar at 100 Pa, calculated with the three-dimensional Monte Carlo model.

potential, the analytical value is higher at low energies ($E<1$ eV) and lower at high energies ($E>1$ eV) (see Fig. 5).

Figure 7 shows the thermalization profiles calculated (1) analytically, (2) with a simplified one-dimensional Monte Carlo model, and (3) with a three-dimensional Monte Carlo model, both assuming the same energy losses as analytically. Also, the thermalization profiles resulting from the three-dimensional Monte Carlo models assuming anisotropic energy losses described by (4) the Molier potential and (5) the power-law potential with power $n=4$ are shown. The models (1) and (2) use the same approximations and hence the agreement is not unexpected. The small differences are due to the completely different way of calculation.

The differences between (2) and (3) reflect the differences between the one-dimensional and the three-dimensional description of the thermalization: the energy losses in both cases are the same, but in the three-dimensional model the atoms not only move forward (away from the cathode) but they can move in all directions due to the three-dimensional scattering. This results in a lower net traveled distance from the cathode and hence a thermalization profile which is slightly more shifted towards the cathode. Comparison of (3) and (4) illustrates that the thermalization profile calculated with the energy losses assumed in the analytical model extends only slightly further into the plasma than the thermalization profile evaluated with the Molier potential. This illustrates that the energy losses used in the analytical model are nearly equal to the energy losses described by the Molier potential, averaged over all energies of importance for the thermalization. The analytical description of the energy-loss process is hence a good approximation for the real situation. Comparison between (4) and (5) shows that the influence of the interaction potential is fairly high, as could also be noticed from Fig. 6. The energy losses calculated with the Molier potential are clearly higher and the thermalization profile is far more concentrated near the cathode than in the case of the power-law potential. The reasonable agreement between (3) and (4) and the large difference between (4) and (5) also indicate that rather high energies ($E>1$ eV) play a more important role in determining the final thermalization profile than the near thermalized energies.

B. Results of the three-dimensional thermalization model

Figure 8 represents the thermalization profile in the cylindrical symmetry, obtained with the three-dimensional model based on the Molier potential, for a Cu/Ar system at a gas pressure of 100 Pa. It can be seen that the majority of the atoms is already thermalized at 1 mm away from the cathode. A section in the axial direction results in Fig. 7, No. 4. In the radial direction, the thermalization profile is fairly constant, except close to the walls where the profile rapidly falls off to zero. Because the thermalization process is determined by the number of elastic collisions of the sputtered atoms with the gas atoms, it will depend strongly on the gas pressure in the discharge, i.e., the thermalization profile will extend further into the plasma at lower pressures. The thermalization process also depends on the masses of sputtered and gas atoms. A larger mass difference between sputtered and gas atoms results in a less efficient energy loss per collision, and hence in a thermalization profile extending deeper into the discharge.

The thermalization model also yields information about the relative amount of atoms that reach the backplate of the cell without being thermalized, the amount of atoms that strike the neck of the cell (see Fig. 1), and the relative amount of backscattering to the cathode. These relative amounts also depend strongly on the gas pressure and the kind of sputtered and gas atoms. As already said, at lower pressure the thermalization profile extends further into the plasma. This means that relatively more sputtered atoms can reach the backplate of the cell without being thermalized. This amount increases linearly as the pressure decreases; for

Cu/Ar the amount is about 0.05% at 1000 Pa, about 0.5% at 100 Pa, and about 5% at 10 Pa. The amount of sputtered atoms that strike the neck of the cell also increases with decreasing pressure, going from about 3.5% at 1000 Pa to about 15% at 100 Pa and about 75% at 10 Pa. The amount of backscattering to the cathode slightly increases with pressure from about 5.5% at 10 Pa to about 8% at 100 Pa and remains constant at higher pressures.

As was also said before, a larger difference between the masses of gas and sputtered atoms results in a thermalization profile penetrating deeper into the plasma. This effect is most clearly seen when the discharge gas is altered. We compared Ar, Ne, and He at 100 Pa and a Cu cathode. In the case of a lighter gas, the thermalization profile extends further into the discharge, resulting in more atoms that reach the backplate of the cell (Ar about 0.4%, Ne about 0.6%, and He about 1.6%), more atoms that strike the neck of the cell (Ar about 15%, Ne about 20%, and He about 50%), and less atoms that scatter back to the cathode (Ar about 8%, Ne about 4%, and He about 0.7%). The influence of the kind of sputtered atoms on their thermalization is not only caused by their mass difference with the discharge gas, but also by the surface binding energy of the atoms in the solid, because this determines the initial energy of the sputtered atoms [see Eq. (7)]. Atoms with a higher surface binding energy enter the plasma with higher energies and will need a longer distance before being thermalized. Comparing Ta and Mo, which have a high atomic mass and also a high surface binding energy (8.1 and 6.82 eV, respectively), with Cu (surface binding energy of 3.49 eV), at an argon pressure of 100 Pa, we find that Ta and Mo have more chance to reach the backplate (both about 0.6%) and the neck of the cell (about 27% and 22%, respectively) and are scattered back to the cathode to a lesser extent (about 3% and 5%, respectively) than Cu (see before).

It is worthwhile to distinguish here backscattering from backdiffusion. Backdiffusion originates from a nonuniform concentration distribution of thermalized sputtered atoms throughout the discharge cell, whereas backscattering deals only with atoms which arrive back at the cathode surface after one or more collisions directly after they are sputtered and without being completely thermalized. The relative amount of backdiffusion is about 70% of the material sputtered from the cathode, as is calculated in Refs. 9 and 21. Backscattering hence contributes only to a minor extent to the total redeposition of sputtered material.

IV. CONCLUSION

A three-dimensional Monte Carlo model has been developed to simulate the thermalization process of the atoms sputtered from the cathode in a glow discharge. Comparison is made with an analytical model described in literature[7,8,10] and the influence of different atom–atom interaction potentials and scattering conditions on quantities related to the thermalization process is evaluated. Use of the power-law potential with power $n=4$ instead of a more accurate Molier potential results in large deviations. The scattering angles calculated are much smaller, resulting in much lower energy losses and hence a thermalization profile extending further in the plasma. Use of a constant energy loss in each scattering event equal to $E\gamma/3$, as was done in the analytical model of Refs. 7, 8, and 10, seems a good approximation to the real energy losses in the thermalization process. The deviation of the one-dimensional analytical model from the three-dimensional Monte Carlo model using a Molier interaction potential is mostly due to the assumption of continuous energy losses along a straight line away from the cathode, instead of taking into account three-dimensional scattering and the possibility of motion in the backward direction.

The Monte Carlo model presented here yields a three-dimensional thermalization profile and gives information about the relative amount of atoms that strike the neck of the discharge cell or reach the backplate without being thermalized and about the relative amount of backscattering. The influence of gas pressure and kind of gas and sputtered atoms is investigated and it is shown that a lower gas pressure, a larger mass difference between sputtered and gas atoms, and a higher surface binding energy of sputtered atoms result in a thermalization profile extending further into the plasma.

ACKNOWLEDGMENTS

A. Bogaerts is indebted to the National Science Foundation (NFWO) for financial support. This research is also sponsored by the Federal Services for Scientific, Technical and Cultural Affairs (DWTC/SSTC) of the Prime Minister's Office through IUAP-III (Conv. 49).

[1] *Glow Discharge Spectroscopies*, edited by R. K. Marcus (Plenum, New York, 1993).
[2] W. W. Harrison, in *Inorganic Mass Spectrometry*, edited by F. Adams, R. Gijbels, and R. Van Grieken (Wiley, New York, 1988).
[3] W. W. Harrison and B. L. Bentz, Prog. Anal. Spectrosc. **11**, 53 (1988).
[4] M. Surendra, D. B. Graves, and G. M. Jellum, Phys. Rev. A **41**, 1112 (1990).
[5] J. P. Boeuf and E. Marode, J. Phys. D **15**, 2169 (1982).
[6] A. Bogaerts, M. van Straaten, and R. Gijbels, Spectrochim. Acta B (in press).
[7] A. Gras-Marti and J. A. Valles-Abarca, J. Appl. Phys. **54**, 1071 (1983).
[8] J. A. Valles-Abarca and A. Gras-Marti, J. Appl. Phys. **55**, 1370 (1984).
[9] M. van Straaten, A. Vertes, and R. Gijbels, Spectrochim. Acta B **46**, 283 (1991).
[10] M. van Straaten, R. Gijbels, and A. Vertes, Anal. Chem. **64**, 1855 (1992).
[11] I. M. Torrens, *Interatomic Potentials* (Academic, New York, 1972).
[12] J. B. Hasted, M. A., and D. Phil., *Physics of Atomic Collisions* (Butterworths, London, 1972).
[13] J. Lindhard, V. Nielsen, M. Scharff, and P. V. Thomsen, Mat. Fys. Medd. Dan. Vid. Selsk. **33**, No. 14 (1963).
[14] J. Lindhard, V. Nielsen, and M. Scharff, Mat. Fys. Medd. Dan. Vid. Selsk. **36**, No. 10 (1968).
[15] K. B. Winterbon, P. Sigmund, and J. B. Sanders, Mat. Fys. Medd. Dan. Vid. Selsk. **37**, No. 14 (1970).
[16] J. Lindhard, M. Scharff, and H. E. Schiøtt, Mat. Fys. Medd. Dan. Vid. Selsk. **33**, No. 14 (1963).
[17] A. Benninghoven, F. G. Rüdenauer, and H. W. Werner, *Secondary Ion Mass Spectrometry* (Wiley, New York, 1987).
[18] VG 9000 Users Manual, Fisons, Winsford, Cheshire CW7 3BX, UK.
[19] J. Sielanko, Radiat. Eff. Lett. **86**, 185 (1984).
[20] Z. Wronski, Vacuum **42**, 635 (1991).
[21] M. van Straaten, Ph.D. thesis, University of Antwerp, 1993.